




## Nonlinear saturation of bubble evolution in a two-dimensional single-mode stratified compressible Rayleigh-Taylor instability

Cheng-Quan Fu <sup>1</sup>, Zhiye Zhao <sup>1,\*</sup>, Xin Xu,<sup>1</sup> Pei Wang,<sup>2</sup>  
Nan-Sheng Liu,<sup>1</sup> Zhen-Hua Wan <sup>1</sup> and Xi-Yun Lu<sup>1</sup>

<sup>1</sup>*Department of Modern Mechanics, University of Science and Technology of China, Hefei, Anhui 230026, People's Republic of China*

<sup>2</sup>*Institute of Applied Physics and Computational Mathematics, Beijing 10094, People's Republic of China*



(Received 21 August 2021; accepted 26 January 2022; published 7 February 2022)

We report nonlinear saturation of bubble evolution occurring in a two-dimensional single-mode stratified compressible Rayleigh–Taylor instability via direct numerical simulation (DNS). A range of Atwood number ( $At = 0.1 \sim 0.9$ ) are tested at varying levels of density stratification, corresponding to a range of static compressibility quantified as a Mach number over  $Ma = 0.1 \sim 1$ . Density stratification is found to cause different bubble behaviors for different  $At$ , with a critical  $At$  of 0.25 at which nonlinear saturation of bubble growth is realized. A modified buoyancy-drag model for stratified compressible RTI is proposed giving an accurate analytical prediction on this DNS-obtained critical  $At$ . Of special interest, similar nonlinear saturation is uncovered for the bubble evolution at  $At = 0.9$  as the pistonlike effect that describes the compressing effects of the rising bubble of light fluid exerting on the heavy fluid ahead of its front is fully extracted. Furthermore, it is demonstrated that the acceleration of the heavy fluid compressed in front of the bubble characterizing the pistonlike effect is nearly constant for different  $Ma$  and its ratio to the external acceleration has a fascinating power law scaling as  $At^{2.5}Ma^2$ .

DOI: [10.1103/PhysRevFluids.7.023902](https://doi.org/10.1103/PhysRevFluids.7.023902)

### I. INTRODUCTION

Rayleigh–Taylor instability (RTI) [1,2] that occurs in the interface where heavy fluid is supported or accelerated by light fluid has a long history in classical hydrodynamics, dating back to the ground-breaking paper of Lord Rayleigh [1]. It has been widely encountered as an important role in natural phenomena and industrial applications where strong compressibility effects are involved, for example, on the flame propagation and development of ignition bubbles in type Ia supernovae, mixing and burning in x-ray bursts, and the inertial confinement fusion [3–7]. Thus, a physical understanding of bubble growth of the compressible RTI is of great significance in manipulating the evolution process of the unstable interface.

Bubble growth in RTI has completely different nonlinear behaviors when subjected to different flow effects, for example, geometry convergence. Intriguing bubble behavior in the nonlinear growth regime, commonly referred to as “nonlinear saturation,” has been obtained analytically for the incompressible RTI of planar and cylindrical geometries. Specifically, the bubbles in the planar RTI are found to have a linear-in-time growth for the nonlinear evolution saturating with a terminal velocity  $V_t = \sqrt{2At/(1+At)(g\lambda/C_d)}$ , where  $At$  is Atwood number;  $g$  is the magnitude of external acceleration  $\mathbf{g}$ ;  $\lambda = 2\pi/k$  is the perturbation wave length with  $k$  being the perturbation wave number; and  $C_d = 6\pi$  and  $2\pi$  for the two- and three-dimensional geometries, respectively. This

\*Corresponding author: [zzy12@ustc.edu.cn](mailto:zzy12@ustc.edu.cn)

saturating terminal velocity derived from the potential flow model [8–13] corresponds in physics to a subtle balance of the buoyancy and drag forces integrated for the growing bubbles, as described by the so-called buoyancy-drag model (BDM) [14–16]. In contrast, a quadratic-in-time growth for the nonlinear bubble evolution has been found in the cylindrical RTI via a delicate analytical model and verified by high-fidelity direction numerical simulation (DNS) [17]. Namely, it means that the bubble growth of cylindrical RTI saturates fascinatingly at a terminal acceleration  $a_b$  that has been formulated as a simplified function of  $g$ ,  $At$ , and  $k$  [17].

Density stratification caused by fluid compressibility is known to have complicated effects on the later-time RTI flows, although its influence on nonlinear bubble evolution has not been well studied. For example, increasing density stratification always stabilizes the single-mode RTI flow and weakens vorticity production via the baroclinic source term [18], while the flow expansion-compression process plays a destabilizing role [19]. For multimode RTI flows, a saturation of the mixing layer thickness is obtained as the density stratification acts to annihilate turbulence production by smoothing the initial density jump [20]. It is indicated that in the compressible RTI the rising bubbles of light fluid act like pistons, compressing the heavy fluid ahead of the fronts. Consequently, shocklets are observed via large eddy simulations [21] as strong compressibility is obtained outside of the mixing layer for  $Ma \simeq 3.0$  and at  $At = 0.533$  and  $0.734$ . However, background density stratification can either suppress or enhance the growth of RTI, depending upon the value of  $At$  defined at the interface [19,22,23]. For an initial condition of thermal equilibrium, the density stratification serves to suppress the RTI growth for a small  $At$ , while for a large  $At$  to enhance the bubble evolution exceeding the nonlinear saturation of the incompressible case.

Motivated by the aforementioned findings, the goal of this work is devoted to the density stratification effects on the bubble evolution in the compressible RTI, with special interest directed to answer the following question: Can similar nonlinear saturation of bubble evolution occur in a stratified compressible RTI? It is of interest whether the bubble growth saturates at velocity or at acceleration if in a manner different from the incompressible cases. To this goal, DNS of two-dimensional single-mode stratified compressible RTI is performed to examine the bubble growth via increasing the density stratification at different Atwood numbers.

## II. NUMERICAL SIMULATIONS

### A. Governing equation and initialization

Following Reckinger *et al.* [22,23], we choose the perturbation wave length ( $\lambda^*$ ), initial pressure ( $p_I^*$ ) and temperature ( $T_I^*$ ) at the interface as the characteristic scales for length, pressure ( $p^*$ ), and temperature ( $T^*$ ), respectively, where the subscript “I” means the quantities at the initial interface and the superscript “\*” means the dimensional physical quantities hereafter. Correspondingly, the density ( $\rho^*$ ) and velocity ( $\mathbf{u}^*$ ) are scaled by  $\rho_I^* = p_I^*(W_h^* + W_l^*)/(2\mathcal{R}^*T_I^*)$  and  $u_I^* = \sqrt{p_I^*/\rho_I^*}$ , respectively, where  $W_h^*$  and  $W_l^*$  represent the molar masses of the heavy and light fluids, respectively, and  $\mathcal{R}^*$  is the universal gas constant. The dimensionless governing equations read as

$$\frac{\partial \rho}{\partial t} + \nabla \cdot (\rho \mathbf{u}) = 0, \quad (1)$$

$$\frac{\partial (\rho \mathbf{u})}{\partial t} + \nabla \cdot (\rho \mathbf{u} \mathbf{u}) = -\nabla p + \frac{1}{\text{Re}} \nabla \cdot \boldsymbol{\sigma} - \text{Ma}^2 \rho \mathbf{e}_y, \quad (2)$$

$$\frac{\partial (\rho e)}{\partial t} + \nabla \cdot [(\rho e + p) \mathbf{u}] = \frac{1}{\text{Re}} \nabla \cdot (\boldsymbol{\sigma} \cdot \mathbf{u} + \mathbf{q}^T + \mathbf{q}^Y) - \text{Ma}^2 \rho \mathbf{u} \cdot \mathbf{e}_y, \quad (3)$$

$$\frac{\partial (\rho Y_m)}{\partial t} + \nabla \cdot (Y_m \mathbf{u}) = \frac{1}{\text{ReSc}} \nabla \cdot (\mu \nabla Y_m), \quad (4)$$

where  $\mathbf{u} = [u, v]$  corresponding to the horizontal ( $x$ ) and vertical ( $y$ ) velocity components, respectively;  $\mathbf{e}_y$  is the unit vector in the  $y$  direction;  $e = C_v T + \mathbf{u} \cdot \mathbf{u}/2$  denotes the specific total energy with  $C_v$  being the specific heats at constant volume;  $Y_m = \rho_m/\rho$  is the species mass fraction with

$m = h, l$  denoting hereafter the heavy and light fluids, respectively. The shear stress tensor is obtained as  $\boldsymbol{\sigma} = 2\mu[\mathbf{S} - (\nabla \cdot \mathbf{u})\boldsymbol{\delta}/3]$ , where  $\mathbf{S}$  is the strain-rate tensor; the viscosity coefficient  $\mu = (T)^{3/2}(1+c)/(T+c)$  is computed by the Sutherland law with  $c = 124\text{K}/T_r^*$  and  $T_r^*$  being the reference temperature;  $\boldsymbol{\delta}$  is the unit tensor. The heat flux  $\mathbf{q}^T = \text{Pr}^{-1}\gamma/(\gamma-1)\kappa\nabla T$  and  $\mathbf{q}^Y = \sum_{m=h,l} C_{pm}T\rho D\text{Sc}^{-1}\nabla Y_m$  account for the thermal diffusion and interspecies mass diffusion, respectively, where  $\kappa$  is the heat conduction coefficient;  $D$  is the diffusion coefficient; and  $\gamma$  is the ratio of specific heats. The fluid properties are defined as linear combinations of the individual species' properties weighted by the mass fractions, for example,  $C_v = \sum_{m=h,l} C_{vm}Y_m$ .

The dimensionless parameters governing the RTI flow are the Mach number  $\text{Ma}$ , the Reynolds number  $\text{Re}$ , the Schmidt number  $\text{Sc}$ , and the Prandtl number  $\text{Pr}$ , defined by

$$\text{Ma} = \sqrt{\frac{g^*\lambda^*}{p_l^*/\rho_l^*}}, \quad \text{Re} = \frac{\rho_l^*U_l^*\lambda^*}{\mu_l^*}, \quad \text{Sc} = \frac{\mu_l^*/\rho_l^*}{D_l^*}, \quad \text{Pr} = C_{pl}^*\frac{\mu_l^*}{\kappa_l^*}, \quad (5)$$

respectively, where  $C_{pl}^*$  is the constant-pressure specific heat at the interface and  $g^*$  is the magnitude of external acceleration. Here, the Mach number is used to characterize the stratified compressibility, i.e., the density stratification [22–24]. The perturbation Reynolds number  $\text{Re}_p$  and Atwood number  $\text{At}$  are defined as

$$\text{Re}_p = \frac{\lambda^*\sqrt{\text{At}/(1+\text{At})g^*\lambda^*}}{\mu_l^*/\rho_l^*}, \quad \text{At} = \frac{W_h^* - W_l^*}{W_h^* + W_l^*}, \quad (6)$$

respectively. The relation between  $\text{Re}_p$  and  $\text{Re}$  is given by  $\text{Re}_p = \sqrt{\text{At}/(1+\text{At})}\text{MaRe}$ .

In this study, we consider the compressible RTI initiated with a hydrostatic equilibrium ( $\mathbf{u} = 0$ ) and a thermal equilibrium ( $T = 1$ ) [22,23,25]. In that, the momentum Eqs. (2) can be reduced to

$$\frac{\partial p^H}{\partial y} = -\text{Ma}^2\rho^H, \quad (7)$$

where  $p^H$  and  $\rho^H$  represent the background pressure and density, respectively. By using of the dimensionless ideal gas equation of state  $p = \rho T/W$ , it yields

$$\rho_h^H = (1 + \text{At}) \exp[-\text{Ma}^2(1 + \text{At})y], \quad \rho_l^H = (1 - \text{At}) \exp[-\text{Ma}^2(1 - \text{At})y]. \quad (8)$$

To smooth the interface density jump, the error function is introduced [22,25]. As shown in Fig. 1(a), a single-mode perturbation,  $I(x) = a_0 \cos(2\pi x)$ , where  $a_0 = 0.02\lambda$  is the dimensionless perturbation amplitude [19] with  $\lambda = 1$  denoting the dimensionless wave length, is introduced at the initially flat interface positioned at  $y = 0$ . Following the recent work [19,22], the computational domain size is set as  $L_x \times L_y = [0, 1] \times [-4, 3]$  for all simulations, which has been verified large enough to obtain the nonlinear behaviors of bubbles. In the present study, we set  $\text{Pr} = 0.72$ ,  $\text{Sc} = 2$ ,  $\gamma = 1.4$ ,  $\text{At} = 0.1 \sim 0.9$ , and  $\text{Ma} = 0.1 \sim 1$ . Figures 1(b)–1(d) show the initial density profiles for various  $\text{Ma}$  and  $\text{At}$ . It is clearly seen in Figs. 1(b)–1(d) that  $\text{At}$  quantifies the density difference between heavy and light fluids at the initial interface and  $\text{Ma}$  determines the strength of density stratification along the vertical direction. As pointed by Wei and Livescu [32], the RTI flow is dominated by diffusive process at a low perturbation Reynolds number  $\text{Re}_p$ . For  $\text{Re}_p \gtrsim 200$ , the RTI flow can be approximated potential at the bubble or spike tips and the velocity of the instability front approaches nonlinear saturation. To this end,  $\text{Re}_p$  is fixed at 1500, high enough for the RTI flow to evolve into the nonlinear stage. Following previous study [26], the bubble height  $H_b$  is calculated as the vertical distance from the unperturbed flat interface positioned at  $y = 0$  to the bubble tip corresponding to a mass fraction value of 99%. As the RTI flows have an unchanged average interface position, i.e., at  $y = 0$  for all  $\text{At}$  and  $\text{Ma}$  considered,  $H_b$  can be regarded as a proper measure of bubble evolution. The bubble velocity is obtained as  $V_b = dH_b/dt$ . In the following discussions, the velocity and time, unless otherwise indicated, are rescaled by  $\sqrt{\text{At}g\lambda^*/(1+\text{At})}$  and  $\tau = \sqrt{\lambda^*/(\text{At}g)}$ , respectively, where the  $g = \text{Ma}^2$  is the amplitude of dimensionless external acceleration.

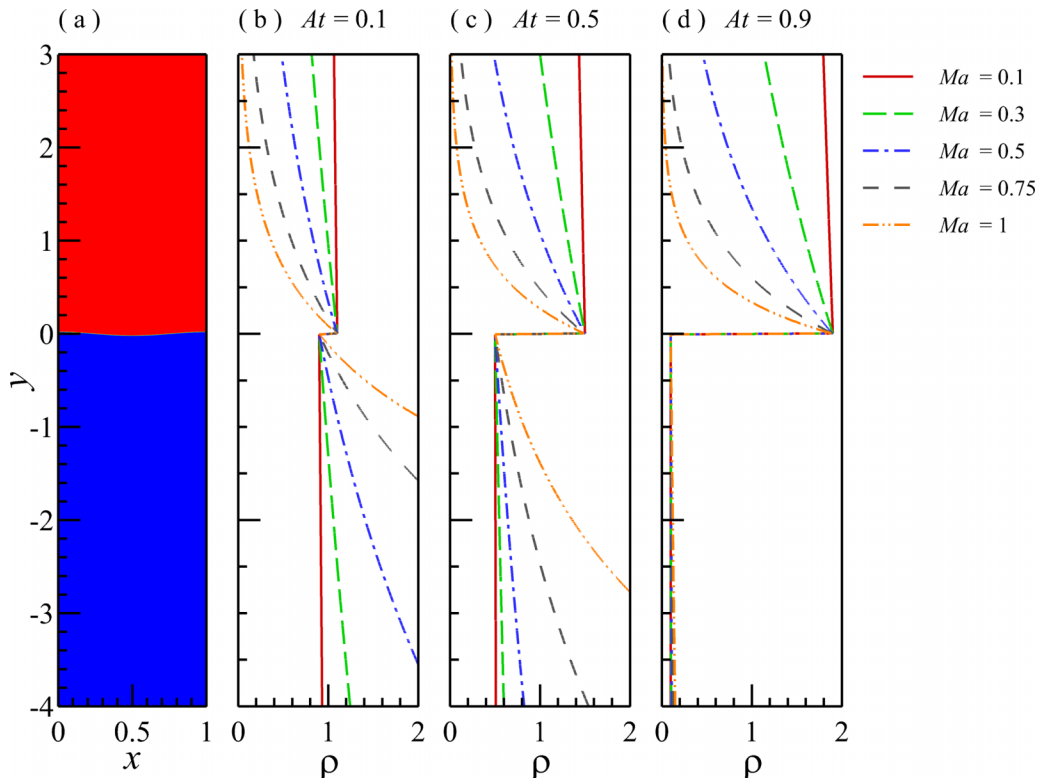


FIG. 1. (a) The computational domain with  $L_x \times L_y = [0, 1] \times [-4, 3]$ . (b–d) The typical density profile of different  $At$  and  $Ma$ .

### B. Numerical method and validation

In the present study, high-fidelity DNS has been performed to solve the governing Eqs. (1)–(4), with the convection terms discretized by the seven-order WENO scheme and the diffusion terms by the six-order central difference scheme, and the third-order Runge-Kutta scheme for the time integration [17,27]. Periodic boundary conditions are applied along the  $x$ -direction and the variables, i.e.,  $\rho$ ,  $u_i$ ,  $e$ , and  $Y_m$ , are fixed at their initialized values at the  $y$ -direction boundaries [19,22,25,28].

To validate the numerical method used, extensive test calculations have been performed and the results obtained are compared to those of previous DNS study on the single-mode compressible RTI [19]. As shown in Fig. 2(a) for typical cases, the bubble growths represented by  $H_b$  of high  $At$  ( $At = 0.9$ ,  $Ma = 0.5$ ) and low  $At$  ( $At = 0.1$ ,  $Ma = 0.1$ ) are in good agreements with those obtained by Luo *et al.* [19]. Thus, the nonlinear bubble behaviors are accurately simulated for various  $At$  and  $Ma$ . Furthermore, the grid resolution used is verified by the converged results obtained by DNS in present study. As the case at  $At = 0.9$  and  $Ma = 1$  is most demanding in grid resolution [19], the converged results depicted in Fig. 2(b) assure that the present simulations are reliable to capture the essential flow dynamics in a single-mode stratified compressible RTI. A mesh size of  $N_x \times N_y = 200 \times 1400$  is used in all the calculations.

### III. RESULTS AND ANALYSIS

Bubble velocity  $V_b$  plotted in Fig. 3 for the typical  $At$  demonstrates the  $At$ -dependent effects of density stratification on the bubble growth, in agreement with the previous findings [19,22,23]. It is seen that for all the  $At$  values considered the bubble evolution has a nonlinear saturation at

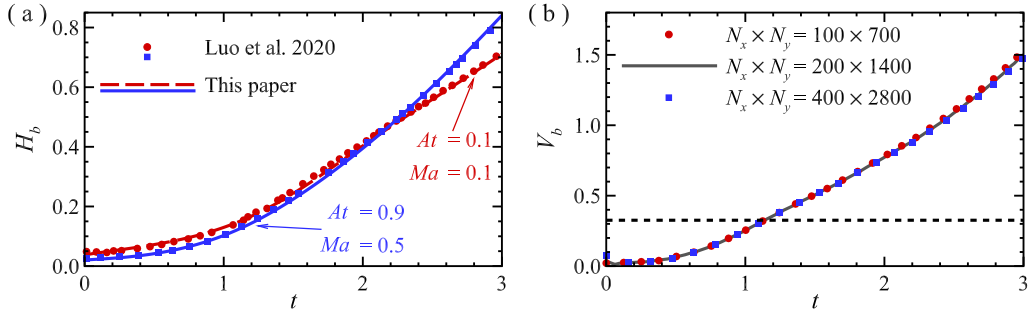


FIG. 2. (a) The bubble height ( $H_b$ ) compared with that obtained by previous study. The (solid or dashed) lines represent the results of our DNS and the symbols (circle or square) represent those of Ref. [19]. (b) Verification of grid resolution used based on the bubble velocity ( $V_b$ ) obtained for  $At = 0.9$  and  $Ma = 1$  by different mesh sizes. The horizontal black dashed line represents the terminal velocity  $V_t$  at which the bubble evolution has a nonlinear saturation in the incompressible RTI.

a low stratification strength ( $Ma = 0.1$ ). Namely,  $V_b$  varies in the nonlinear regime ( $t \gtrsim 1.8$ ) with nearly a plateau value close to the terminal velocity  $V_t$  of the incompressible RTI. Intriguingly, there exists a moderate value of  $At = 0.25$  at which the nonlinear saturation of bubble growth is observed similar to the incompressible RTI, namely, the density stratification effects on the bubble evolution are almost trivial, and a slight change is found for  $V_b$  as  $Ma$  varies from 0.1 to 1 [see Fig. 3(b)]. However, at a smaller  $At$  (of 0.1),  $V_b$  obtains a marked decrease when  $t \gtrsim 1.8$  after an exponential increase in the linear regime ( $t \lesssim 1.8$ ). This trend of  $V_b$  becomes more remarkable as  $Ma$  increases from 0.1 up to 1, indicating an enhanced decelerating effect on the nonlinear bubble evolution induced by density stratification [see Fig. 3(a)]. In contrast, at a larger  $At$  (of 0.9),  $V_b$  obtains a continuous increase versus  $t$  for  $Ma = 0.1 \sim 1$ , indicating an accelerating effect which increases significantly due to the enhanced density stratification [see Fig. 3(c)]. Similar to the finding of Luo *et al.* [19], a nearly linear-in-time growth of  $V_b$  is demonstrated in the nonlinear regime at  $At = 0.9$ , especially for high  $Ma$  of 0.75 and 1. The linearly dependent coefficients of  $Ma = 0.75$  and 1.0 are obtained as 0.999 and 0.993, respectively.

The occurrence of nonlinear saturation of bubble growth at  $At = 0.25$  for different  $Ma$  can be explained by an extension of the classical BDM [14,15,29] to the stratified compressible RTI. Different from the classic BDM proposed for incompressible RTI [14,15,29], density stratification effects have to be accounted for in the present study when taking integration for the growing bubble to obtain the inertial ( $f_i$ ), buoyancy ( $f_b$ ), and drag ( $f_d$ ) forces that appear in sequence in the following

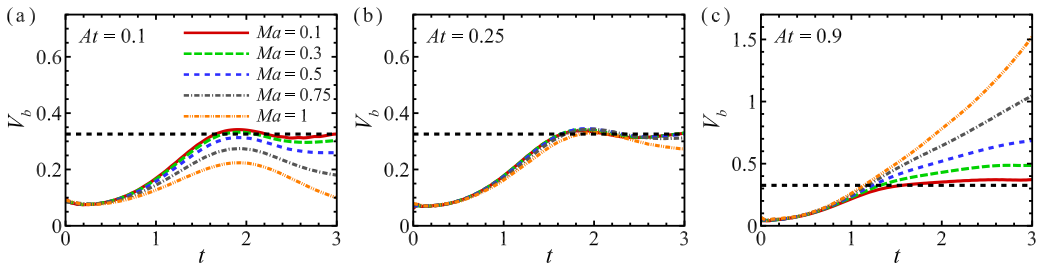


FIG. 3. Bubble growth versus time depicted by the bubble velocity  $V_b$  for (a)  $At = 0.1$ , (b)  $At = 0.25$ , and (c)  $At = 0.9$ . The horizontal black dashed line in each panel represents the bubble terminal velocity  $V_t$  of the incompressible RTI.

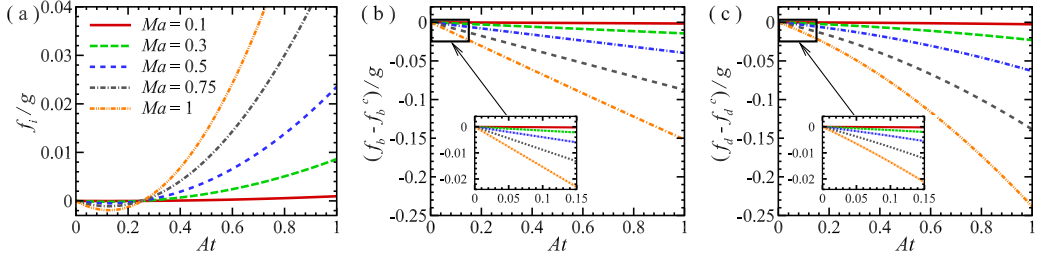


FIG. 4. (a) The inertia force  $f_i$  evaluated by the modified BDM using the initialized density fields of stratified RTI. (b) The difference between the modified buoyancy ( $f_b$ ) and the buoyancy ( $f_b^c$ ) of the classic BDM for the unstratified RTI. (c) The difference between modified drag ( $f_d$ ) and the drag ( $f_d^c$ ) of the classic BDM for the unstratified RTI. Here, all forces rescaled by  $g$  are evaluated under an assumption that the bubble growth has  $V_b = V_t$  as the nonlinear saturation is realized with roughly  $\eta_b = 0.1\lambda$  [14,31–33].

modified BDM,

$$(\bar{\rho}_l + C_a \bar{\rho}_h) \frac{dV_b}{dt} = (\bar{\rho}_h - \bar{\rho}_l)g - \hat{\rho}_h C_d \frac{V_b^2}{\lambda}. \quad (9)$$

Here,  $C_a = 2$  for 2D,  $\bar{\rho}_h = V^{-1} \int_V \rho_h dV$  and  $\bar{\rho}_l = V^{-1} \int_V \rho_l dV$  are the volume-averaged densities for the heavy and light fluids that are set in motion by the rising bubble of volume  $V$ , and  $\hat{\rho}_h = S^{-1} \int_S \rho_h dS$  is the area-averaged density for the heavy fluid over the bubble interface of area  $S$ . According to the classical BDM, bubble rising occurs as the buoyancy force is greater than the drag force that comes from the interaction between the rising bubble and the heavy fluid ahead of its front [14,15,29,30]. In that, the quantities in the modified BDM are integrated according to the above physical interpretations of the corresponding force terms in Eq. (9). Inspired by Goncharov [11], Layzer [8], Zhang [9], the shape of bubble interface is approximated as a dimensionless parabolic profile,  $y_b = [-16x^2 + 1]\eta_b$ , which has a peak located at the bubble tip  $(0, \eta_b)$  and two intersections with the unperturbed interface, i.e.,  $(0.25, 0)$  and  $(-0.25, 0)$  due to the  $x$ -periodic condition. By using the initially stratified density fields given in Eq. (8), the modified BDM yields the inertial force  $f_i$  as depicted in Fig. 4(a) for various  $At$  and  $Ma$ , providing that the bubble growth saturates when  $V_b = V_t$  and roughly  $\eta_b = 0.1\lambda$  [14,31–33]. It is clearly demonstrated that a critical Atwood number ( $At \approx 0.25$ ) is obtained for  $0.1 \leq Ma \leq 1$ , at which the inertial force  $f_i$  has a zero value as  $f_b$  is balanced by  $f_d$  and the nonlinear saturation is realized for the bubble growth as expected [see Fig. 3(b)]. To further interpret the nonlinear behaviors of bubble velocity in stratified RTI, the buoyancy ( $f_b^c$ ) and drag ( $f_d^c$ ) forces of the classic BDM for the unstratified RTI are also evaluated, and the force differences, i.e.,  $f_b - f_b^c$  and  $f_d - f_d^c$ , are shown in Figs. 4(b). It is clearly seen in Figs. 4(b) and 4(c) that  $f_b$  and  $f_d$  are reduced as compared to their counterparts in the unstratified RTI, leading to different behaviors in nonlinear bubbles' evolution between the unstratified and stratified RTI. Specifically, for large  $At > 0.25$ , a positive inertial force corresponding to an accelerating bubble velocity is obtained [see Fig. 4(a)], resulting from that the buoyancy force has a decrease extent much smaller than that of the drag force [see Figs. 4(b) and 4(c)]. While for small  $At < 0.25$ , an opposite situation is obtained as shown clearly in Figs. 4(a)–4(c). The above predictions are in excellent agreement with what illustrated in Fig. 3 by the bubble velocity  $V_b$  obtained from the present DNS calculations. Furthermore, the procedure described above for the 2D bubble can be applied to its 3D counterpart to obtain the critical Atwood number. Specifically, taking the  $y$  axis as the direction of the density gradient and assuming a cylindrical symmetry for the 3D bubble [11], the shape of 3D bubble interface can be approximated to have an axisymmetric parabolic surface, i.e.,  $y_b = [-16(x^2 + z^2) + 1]\eta_b$ , which has a peak located at the bubble tip  $(0, \eta_b, 0)$  and the intersecting curved line  $x^2 + z^2 = 0.25^2$  within the unperturbed interface at  $y = 0$ . Similar to the cases of 2D bubble, the modified BDM yields the inertial force  $f_i$  for the 3D bubbles as depicted

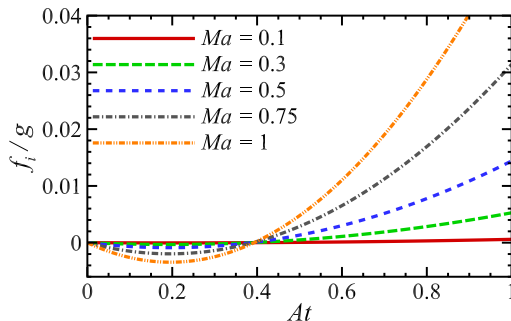


FIG. 5. The inertia force  $f_i$  evaluated by the modified BDM as given in Eq. (9), providing that the bubble growth saturates with  $V_b = V_i$  and roughly  $\eta_b = 0.1\lambda$  in the 3D RTI. Here,  $f_i$  is rescaled by  $g$ .

in Fig. 5 for various  $At$  and  $Ma$ , obtaining a critical Atwood number ( $At \approx 0.4$ ) for the 3D stratified compressible RTI in the range of  $0.1 \leq Ma \leq 1$ .

According to Olson and Cook [21], the rising bubble of light fluid acting like a piston in a stratified compressible RTI compresses the heavy fluid ahead of its front, resulting in a sharp increase of the density, pressure, and velocity in the heavy fluid region especially when the density stratification is sufficiently strong [22]. To confirm this pistonlike effect, the vertical velocity  $v$  profiles along the vertical lines across the bubble ( $x = 0$ ) and spike tips ( $x = 0.5$ ) for the cases of weak ( $Ma = 0.1$ ) and strong ( $Ma = 1$ ) density stratification are plotted in Figs. 6(a) and 6(d). For the case of  $Ma = 1$  [see Fig. 6(d)], the vertical velocities  $v$  at both  $x = 0$  and  $x = 0.5$  have a same plateau value in front of the rising bubble at time  $t = 3.0$ , resulting from the compressing effects of the rising bubble on heavy fluid. In contrast, for the case of  $Ma = 0.1$ , the heavy fluid ahead of the rising bubble remains almost the hydrostatic equilibrium, indicating that the pistonlike effect is negligible due to the weak density stratification.

To illustrate this pistonlike effect of rising bubble, the Helmholtz decomposition [34] are employed to the velocity field, i.e.,

$$\mathbf{u} = \mathbf{u}^s + \mathbf{u}^c, \quad (10)$$

where  $\mathbf{u}^s = [u^s, v^s]$  and  $\mathbf{u}^c = [u^c, v^c]$  are the solenoidal and compressive (irrotational) components respectively. Two intriguing flow physics are indicated by the contour plots of  $v^c$  and  $v^s$  shown in Figs. 6(b) and 6(c) and 6(e) and 6(f) for the cases of  $Ma = 0.1$  and 1, respectively. First, it is clearly seen that for the case of  $Ma = 1$  the vertical velocity  $v$  plateau ahead of the rising bubble is mainly caused by the vertical compressive velocity  $v^c$ , whereas the heavy fluid motion is induced by the great compressing effect exerted by the rising bubble, i.e., dominated by the pistonlike effect. However, for the case of  $Ma = 0.1$ , the  $v^c$  value is almost zero in front of the rising bubble due to that the flow compression is negligible for the RTI with weak density stratification. Second, it is noted that the vertical solenoidal velocity  $v^s$  is dominant to  $v$  near the spike interface for both the cases of  $Ma = 0.1$  and  $Ma = 1$ , namely, it accounts for the peak (rising) and valley (falling) values of  $v$  occurring at  $x = 0$  and  $0.5$ , respectively, across the mushroom caps of the spike interface [see Figs. 6(a) and 6(d)]. This observation is also obtained for the unstratified RTI [33], which has been interpreted due to that the heavy (falling) and light (rising) fluid motions near the spike are dominated by the intense shearing process. In that, the fluid motions near the spike in stratified compressible RTI result from the shearing process other than the density stratification. As known for the unstratified RTI at high  $At$ , such an intense shearing process results in the Kelvin-Helmholtz roll-up effect and generates baroclinic vorticity near the spike tip [33], which in turn induces the peak value of  $v$  near the rolled-up spike interface.

Based on the above analysis, the nonlinear bubble growth is revisited in the following by extracting this pistonlike effect which can be characterized by the velocity of the compressed heavy

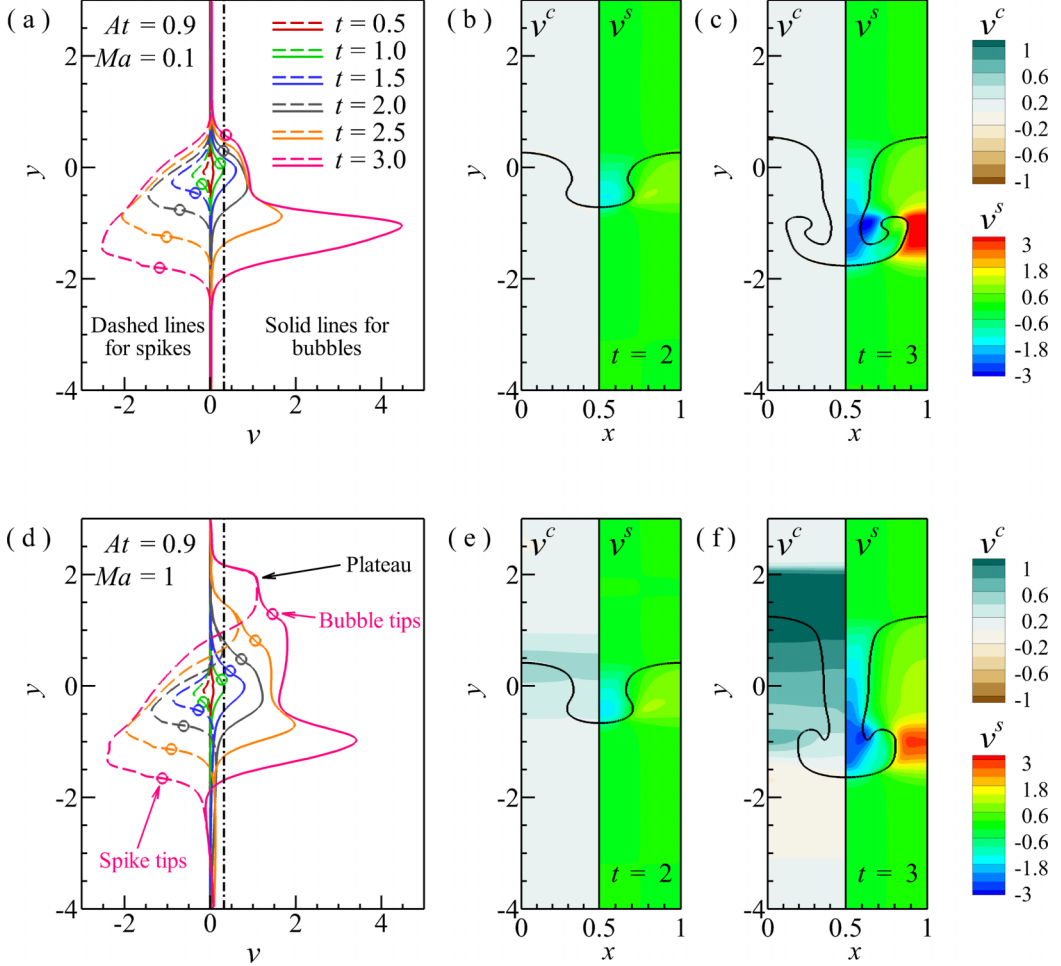


FIG. 6. The  $v$  profiles (a, d) along the vertical lines across the bubble ( $x = 0$ , denoted by the solid lines) and spike ( $x = 0.5$ , denoted by the dashed lines) tips, and the contour plots (b, c, e, f) of the compressive ( $v^c$ , left half) and solenoidal ( $v^s$ , right half) components of vertical velocity  $v$ , for  $At = 0.9$ ,  $Ma = 0.1$  (a–c) and  $At = 0.9$ ,  $Ma = 1$  (d–f). The vertical black dashed lines in panels (a) and (d) represent the bubble terminal velocity  $V_t$  of the incompressible RTI. The circles marked on the  $v$  profile denote the vertical position of the bubble and spike tips at each moment. The dark lines in panels (b, c) and (e, f) represent the heavy/light fluid interface where  $Y_h = 0.5$ .

fluid ahead of the rising bubble,  $V_p$ , obtained as

$$V_p = \frac{1}{L_x} \int_0^{L_x} v(x, y_p) dx. \quad (11)$$

In the above equation,  $y_p$  is the  $y$  position at which the heavy fluid above two neighboring bubbles at  $x = 0.5$  [the dashed lines in Fig. 6(d)] has a peak value of  $v$ , i.e., the  $v$  value of the plateau when appearing in front of the rising bubble. It is indicated in Figs. 7(a) and 7(b) that the pistonlike effect becomes more important only in the nonlinear regime. Specifically, for the critical  $At$  of 0.25 the pistonlike effect is quite weak as  $V_p$ , despite of its continuous increase versus  $Ma$ , obtains a very small value compared to the terminal velocity  $V_t$  of the incompressible RTI [see Fig. 7(a)]. This terminal velocity  $V_t$  is exceeded obviously by  $V_p$  due to its great nearly linear growth occurring in



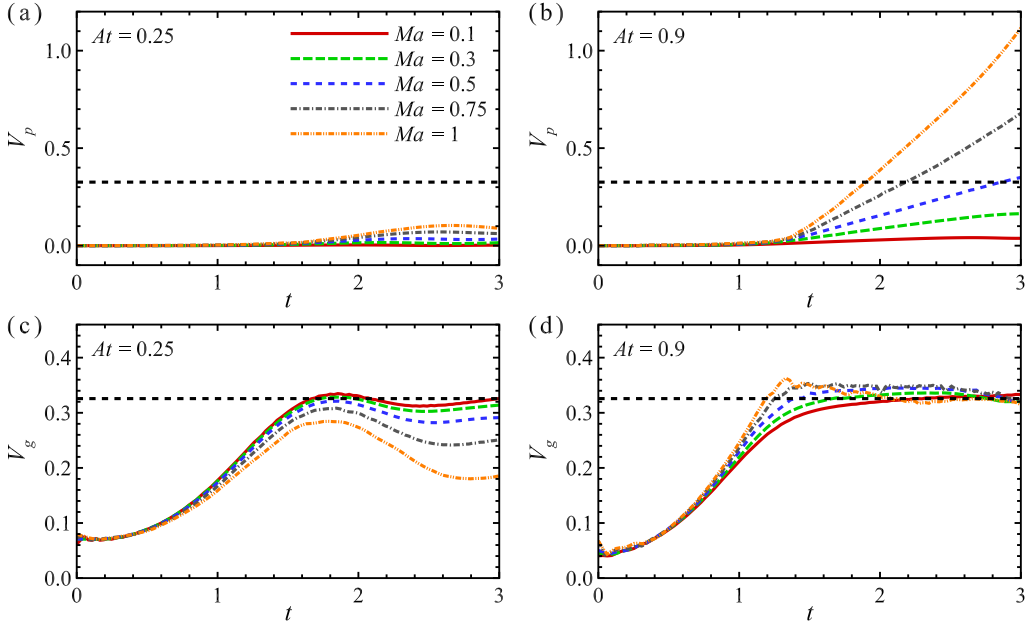


FIG. 7. The velocity  $V_p$  of the compressed heavy fluid ahead of the rising bubble versus time at (a)  $At = 0.25$  and (b)  $At = 0.9$ . The bubble penetration velocity  $V_g$  versus time at (c)  $At = 0.25$  and (d)  $At = 0.9$ . Here, the velocity  $V_p$  is scaled by  $\sqrt{At/(1+At)g\lambda}$ , while the bubble penetration velocity  $V_g$  is scaled by  $\sqrt{At/(1+At)(g+a_p)\lambda}$ . The horizontal black dashed line in each panel represents the bubble terminal velocity  $V_t$  of the incompressible RTI.

the nonlinear regime at  $At = 0.9$  especially for  $Ma = 0.75$  and  $1$  [see Fig. 7(b)]. Note that, the nearly linear growth of  $V_p$  when  $t > 1.2$  for all  $Ma$  corresponds to an almost constant acceleration  $a_p = dV_p/dt$ , which can be viewed as an additional characterization of the pistonlike effect originated in the density stratification.

Following Betti and Sanz [35], a bubble penetration velocity  $V_g = V_b - V_p$  is defined to examine the nonlinear bubble evolution with the pistonlike effect extracted fully. As mentioned by Zhou [5], both the gravitational field pointing from heavy to light fluid and the interface acceleration pointing from light to heavy fluid can initiate the growth of the RTI. There is of course equivalence between gravity and acceleration [5]. These two factors work near the rising bubble tips for the present stratified compressible RTI. Specifically, the rising bubbles compress the heavy fluid in front of it, causing the heavy fluid to move with the bubble at its acceleration  $a_p$  which points from light fluid to heavy fluid. To this end, the effective gravity driving the bubble growth in compressible RTI is equivalent to  $g + a_p$ . Thus,  $V_g$  obtained for the typical cases of  $At = 0.25$  and  $0.9$  are plotted in Figs. 7(c) and 7(d), rescaled by  $\sqrt{At/(1+At)(g+a_p)\lambda}$  corresponding to an extraction of the acceleration  $a_p$ . It is seen that when the pistonlike effect is extracted,  $V_g$  of  $At = 0.25$  demonstrates a bubble evolution reminiscent of that of  $At = 0.1$  [see Fig. 3(a)], growing exponentially in the linear regime and decreasing markedly in the subsequent nonlinear regime [see Fig. 7(c)]. It means that the nonlinear saturation of bubble growth at  $At = 0.25$  for the stratified compressible RTI is realized by virtue of the pistonlike effect. Of crucial interest, the penetration velocity  $V_g$  of  $At = 0.9$  for all  $Ma$  also saturates roughly in the nonlinear regime, namely, when  $t > 1.5$  it evolves into nearly a plateau value quite close the terminal velocity  $V_t$  of the incompressible RTI [see Fig. 7(d)]. This observation indicates that the bubble evolution of the stratified compressible RTI at  $At = 0.9$  can be approximated as a superimposition of the pistonlike effect induced by density stratification on its counterpart of the incompressible RTI. Taken together with  $V_b$  shown in Fig. 3, the variations of

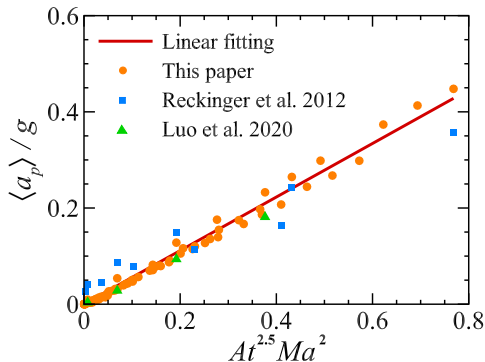


FIG. 8. A scaling law fitted for the ratio of the compressed heavy fluid acceleration  $\langle a_p \rangle$  averaged over  $1.5 < t < 3.0$  to external acceleration  $g$  for various  $At$  and  $Ma$ . The red line corresponds to the linear fitting of the data (orange circle) obtained in the present simulations for  $0.1 \leq At \leq 0.9$  and  $0.1 \leq Ma \leq 1$ , where the slope is 0.557 and the linearly dependent coefficient is 0.993. The blue square and green Delta denote the data obtained by Reckinger *et al.* [22] ( $At = 0.7, 0.9$  and  $0.1 \leq Ma \leq 1$ ) and Luo *et al.* [19] ( $At = 0.9$  and  $0.1 \leq Ma \leq 0.7$ ), respectively.

$V_p$  and  $V_g$  in Fig. 7 point to the following flow physics. For a low  $At < 0.25$ , the nonlinear bubble evolution (namely,  $V_b$ ) is dominated mainly by the bubble penetration velocity  $V_g$  which is generated by the buoyancy force like in the incompressible RTI and gets suppressed due to the density stratification. Whereas for a high  $At > 0.25$ ,  $V_b$  is dominated by the velocity  $V_p$  characterizing the pistonlike effect that becomes more significant versus increasing  $Ma$ .

The next examination is devoted to the acceleration  $a_p$  of the compressed heavy fluid ahead of the rising bubble. Enlightened by the nearly constant  $a_p$  indicated by Figs. 7(a) and 7(b) in the nonlinear regime, we attempt to propose a scaling law to quantitatively describe the averaged  $a_p$  when  $1.5 < t < 3.0$ , i.e.,  $\langle a_p \rangle$ , for all the  $At$  and  $Ma$  considered. As the pistonlike effect is attributed to the rising bubble acting like a piston to compress the heavy fluid ahead of its front, it is naturally expected that  $\langle a_p \rangle$  can be formulated as a function of the compressibility of the heavy fluid that is characterized by  $Ma$  and the buoyancy driving the rising bubble that is determined by  $At$  and  $g$ . Specifically, a scaling law of  $\langle a_p \rangle$  could be obtained as  $At^\alpha Ma^\beta$ , when rescaled by  $g$ . By the fitting test for the calculating results, it is found that when  $\alpha = 2.5$  and  $\beta = 2$ ,  $\langle a_p \rangle / g$  agrees well with a linear growth versus  $At^{2.5} Ma^2$ , and the linearly dependent coefficient is high up to  $\sim 0.993$ . In other words, the ratio of  $\langle a_p \rangle$  to  $g$  scales as a power law of  $At^{2.5} Ma^2$  based on our numerical results, as shown in Fig. 8. The data obtained by Reckinger *et al.* [22] and Luo *et al.* [19] are also plotted in Fig. 8, which confirms this power law of  $\langle a_p \rangle$ .

#### IV. CONCLUDING REMARKS

In summary, nonlinear saturation of bubble evolution occurring in a single-mode stratified compressible RTI has been reported via DNS. Specifically, nonlinear saturation of bubble growth is found to be realized alike to the incompressible RTI at a critical  $At$  ( $\approx 0.25$ ) when the Mach number  $Ma$  quantifying the density stratification varies from 0.1 to 1. A modified buoyancy-drag model is proposed to account for the density stratification effects, which gives an accurate prediction of the above critical  $At$  value analytically. Of special interest, a similar nonlinear saturation is uncovered for the nonlinear bubble evolution at a high Atwood number ( $At = 0.9$ ), as the so-called pistonlike effect exerted by the rising bubble of light fluid to compress the heavy fluid ahead of its front is extracted fully. It is found that at a lower  $At (< 0.25)$ , the nonlinear bubble evolution is dominated mainly by the buoyancy force which is the sole mechanism to facilitate the bubble growth in the incompressible RTI even gets suppressed here due to density stratification, and at a

higher  $At (> 0.25)$  by the pistonlike effect that acts like a piston to compress the heavy fluid ahead of the rising bubble and induces great acceleration for the nonlinear bubble growth especially for the high  $Ma$  cases. Furthermore, it is demonstrated that the acceleration of the compressed heavy fluid ahead of the rising bubble, as an additional characterization of the pistonlike effect, is nearly constant for different  $Ma$  and its ratio to the external acceleration has a fascinating power law scaling as  $At^{2.5}Ma^2$ .

#### ACKNOWLEDGMENTS

The authors are very grateful to Dr. Y. S. Zhang at the Institute of Applied Physics and Computational Mathematics for technical support. This work was supported by the Natural Science Foundation of China (No. 11621202 and No. 92052301), the Science Challenge Project (No. TZ2016001), the Fundamental Research Funds for the Central Universities, and the USTC Research Funds of the Double First-Class Initiative.

---

- [1] Lord Rayleigh, Investigation of the character of the equilibrium of an incompressible heavy fluid of variable density, *Proc. R. Math. Soc.* **s1-14**, 170 (1882).
- [2] G. I. Taylor, The instability of liquid surfaces when accelerated in a direction perpendicular to their planes. I, *Proc. R. Soc. London A* **201**, 192 (1950).
- [3] J. Nuckolls, A. Thiessen, L. Wood, and G. Zimmerman, Laser compression of matter to super-high densities: Thermonuclear (CTR) applications, *Nature (London)* **239**, 139 (1972).
- [4] A. Burrows, Supernova explosions in the universe, *Nature (London)* **403**, 727 (2000).
- [5] Y. Zhou, Rayleigh–Taylor and Richtmyer–Meshkov instability induced flow, turbulence, and mixing. I, *Phys. Rep.* **720-722**, 1 (2017).
- [6] Y. Zhou, Rayleigh–Taylor and Richtmyer–Meshkov instability induced flow, turbulence, and mixing. II, *Phys. Rep.* **723-725**, 1 (2017).
- [7] H. Zhang, R. Betti, R. Yan, and H. Aluie, Nonlinear bubble competition of the multimode ablative Rayleigh–Taylor instability and applications to inertial confinement fusion, *Phys. Plasmas* **27**, 122701 (2020).
- [8] D. Layzer, On the instability of superposed fluids in a gravitational field, *Astrophys. J.* **122**, 1 (1955).
- [9] Q. Zhang, Analytical Solutions of Layzer-Type Approach to Unstable Interfacial Fluid Mixing, *Phys. Rev. Lett.* **81**, 3391 (1998).
- [10] K. O. Mikaelian, Analytic Approach to Nonlinear Rayleigh–Taylor and Richtmyer–Meshkov Instabilities, *Phys. Rev. Lett.* **80**, 508 (1998).
- [11] V. N. Goncharov, Analytical Model of Nonlinear, Single-Mode, Classical Rayleigh–Taylor Instability at Arbitrary Atwood Numbers, *Phys. Rev. Lett.* **88**, 134502 (2002).
- [12] K. O. Mikaelian, Explicit expressions for the evolution of single-mode Rayleigh–Taylor and Richtmyer–Meshkov instabilities at arbitrary Atwood numbers, *Phys. Rev. E* **67**, 026319 (2003).
- [13] Q. Zhang and W.-X. Guo, Universality of finger growth in two-dimensional Rayleigh–Taylor and Richtmyer–Meshkov instabilities with all density ratios, *J. Fluid Mech.* **786**, 47 (2016).
- [14] U. Alon, J. Hecht, D. Ofer, and D. Shvarts, Power Laws and Similarity of Rayleigh–Taylor and Richtmyer–Meshkov Mixing Fronts at All Density Ratios, *Phys. Rev. Lett.* **74**, 534 (1995).
- [15] Y. Srebro, Y. Elbaz, O. Sadot, L. Arazi, and D. Shvarts, A general buoyancy-drag model for the evolution of the Rayleigh–Taylor and Richtmyer–Meshkov instabilities, *Laser Part. Beams* **21**, 347 (2003).
- [16] P. Ramaprabhu, V. Karkhanis, R. Banerjee, H. Varshochi, M. Khan, and A. G. W. Lawrie, Evolution of the single-mode Rayleigh–Taylor instability under the influence of time-dependent accelerations, *Phys. Rev. E* **93**, 013118 (2016).
- [17] Z.-Y. Zhao, P. Wang, N.-S. Liu, and X.-Y. Lu, Analytical model of nonlinear evolution of single-mode Rayleigh–Taylor instability in cylindrical geometry, *J. Fluid Mech.* **900**, A24 (2020).

- [18] M. A. Lafay, B. L. Creurer, and S. Gauthier, Compressibility effects on the Rayleigh–Taylor instability between miscible fluids, *Europhys. Lett.* **79**, 64002 (2007).
- [19] T.-F. Luo, J.-C. Wang, C.-Y. Xie, M.-P. Wan, and S.-Y. Chen, Effects of compressibility and Atwood number on the single-mode Rayleigh–Taylor instability, *Phys. Fluids* **32**, 012110 (2020).
- [20] S. Gauthier, Compressibility effects in Rayleigh–Taylor flows: Influence of the stratification, *Phys. Scr.* **T155**, 014012 (2013).
- [21] B. J. Olson and A. W. Cook, Rayleigh–Taylor shock waves, *Phys. Fluids* **19**, 128108 (2007).
- [22] S. J. Reckinger, D. Livescu, and O. V. Vasilyev, Simulations of compressible Rayleigh–Taylor instability using the adaptive wavelet collocation method, in *Proceedings of the 7th International Conference on Computational Fluid Dynamics (ICCFD7)*, Big Island, Hawaii (2012).
- [23] S. J. Reckinger, D. Livescu, and O. V. Vasilyev, Comprehensive numerical methodology for direct numerical simulations of compressible Rayleigh–Taylor instability, *J. Comput. Phys.* **313**, 181 (2016).
- [24] D. Livescu, Compressibility effects on the Rayleigh–Taylor instability growth between immiscible fluids, *Phys. Fluids* **16**, 118 (2004).
- [25] Z.-X. Hu, Y.-S. Zhang, B.-L. Tian, Z.-W. He, and L. Li, Effect of viscosity on two-dimensional single-mode Rayleigh–Taylor instability during and after the reacceleration stage, *Phys. Fluids* **31**, 104108 (2019).
- [26] S. A. Wieland, P. E. Hamlington, S. J. Reckinger, and D. Livescu, Effects of isothermal stratification strength on vorticity dynamics for single-mode compressible Rayleigh–Taylor instability, *Phys. Rev. Fluids* **4**, 093905 (2019).
- [27] Z.-Y. Zhao, N.-S. Liu, and X.-Y. Lu, Kinetic energy and enstrophy transfer in compressible Rayleigh–Taylor turbulence, *J. Fluid Mech.* **904**, A37 (2020).
- [28] Z.-X. Hu, Y.-S. Zhang, and B.-L. Tian, Evolution of Rayleigh–Taylor instability under interface discontinuous acceleration induced by radiation, *Phys. Rev. E* **101**, 043115 (2020).
- [29] H. Takabe and A. Yamamoto, Reduction of turbulent mixing at the ablation front of fusion targets, *Phys. Rev. A* **44**, 5142 (1991).
- [30] G. Dimonte, Spanwise homogeneous buoyancy-drag model for Rayleigh–Taylor mixing and experimental evaluation, *Phys. Plasmas* **7**, 2255 (2000).
- [31] J. Hecht, U. Alon, and D. Shvarts, Potential flow models of Rayleigh–Taylor and Richtmyer–Meshkov bubble fronts, *Phys. Fluids* **6**, 4019 (1994).
- [32] T. Wei and D. Livescu, Late-time quadratic growth in single-mode Rayleigh–Taylor instability, *Phys. Rev. E* **86**, 046405 (2012).
- [33] X. Bian, H. Aluie, D.-X. Zhao, H. Zhang, and D. Livescu, Revisiting the late-time growth of single-mode Rayleigh–Taylor instability and the role of vorticity, *Physica D* **403**, 132250 (2020).
- [34] J.-C. Wang, Y.-T. Yang, Y.-P. Shi, Z.-L. Xiao, X.-T. He, and S.-Y. Chen, Cascade of Kinetic Energy in Three-Dimensional Compressible Turbulence, *Phys. Rev. Lett.* **110**, 214505 (2013).
- [35] R. Betti and J. Sanz, Bubble Acceleration in the Ablative Rayleigh–Taylor Instability, *Phys. Rev. Lett.* **97**, 205002 (2006).